ISSN (Print): 2476-8316
ISSN (Online): 2635-3490
Dutse Journal of Pure and Applied Sciences (DUJOPAS), *Vol. 6 No. 3 September 2020*

Study on Optical Properties and Surface Morphology of PbS Nanostructure Prepared by Microwave Irradiation Synthesis

N M Maharaz[1*], Y Tijjani [2], Nasir I Fagge[3], Abdullahi Usman[4] , Auwalu Inusa Abubakar[4]

[1]Department of Physics,
Federal University Dutse,
Jigawa State, Nigeria

[2]Department of Mechanical Engineering,
Bayero University,
Kano, Nigeria

[3]Department of Physics,
Bayero University,
Kano, Nigeria

[4]Department of Physics,
Kano University of Science and Technology,
Wudil.

E-mail: nmaharaz@gmail.com

Abstract

Different particle sizes with cubic structure of PbS nanocrystals were synthesized using microwave irradiation method from lead acetate and thioacetamide as starting materials and ethylene glycol used as solvents. A 300W oven operating at 20% of the nominal power in periods of different irradiation time was employed. The obtained dispersions were analysed by X-rays diffraction (XRD), transmission electron microscopy (TEM), Field emission scanning electron microscopy (FESEM) and UV-VIS Spectroscopy. The surfaces morphology of each sample was changed apparently with increases in irradiation time.From the UV absorption, a strong blue-shift with decreasing in nanoparticles size was obtained, which is clearly explained by quantum confinement effect of the PbS nanoparticles. This result clearly shows that a longer irradiation time influences Ostwald ripening due to its effect on the interfacial energy, growth rate coefficients, and solubility which can increase the particle size.

Keywords: Lead sulfide; Nanostructure; Microwave Irradiation; Morphology; Optical Properties

**Author for Correspondence*

INTRODUCTION

Synthesis of semiconductor nanostructure has become an important research line in the recent years due to the strong dependency of the size of the material particles over their properties: optical, mechanical and electrical(Lai *et al.*, 2012).Nanocrystals semiconductor possesses various unique properties, that vary from those of corresponding bulk materials due to three-dimensional confinement of electrons and holes in a small volume or the fact that the number of atoms on the surface is more comparable to that inside the particles(Kus *et al.*, 2018; Wise, 2000). The surface of a nanoparticle is more relevant than the bulk as regards its properties, as nanoparticles have a larger surface-to-volume ratios. Surface atoms are bound by weaker forces because of missing neighbours, which leads to high surface reactivity. The surface is at the stage on which chemical reaction, sublimation, adsorption, desorption, etc occur. For that, there has been much interest in developing semiconductor nanoparticles (Gomez and Tigli, 2013; Rai *et al.*, 2013). They can be prepared in the form of dispersed colloids (Yamamoto and Kuroda, 2016) or trapped and stabilized within micelles (Singh and Mohanty, 2015), polymers (Kango *et al.*, 2013), zeolites (Peng *et al.*, 2015), or glass (Taglietti *et al.*, 2014). In some cases, nanoparticles prepared by these techniques have poorly surfaces exterior and a relatively broad size distribution. Microwave irradiation as a heating process, which is extensively quite, quick, uncomplicated and efficient in energy, has been advanced and is generally used in various research fields(Fuku *et al.*, 2013). It is generally known that dielectric heating is generated due to the interaction of dielectric materials, liquid or solid with microwave. Electric dipoles present in dielectric substances respond to the applied electric field. In polar solvents, this permanent reorientation causes friction between entire molecules, which finally generate heat. Claimed effects of microwave irradiation consist thermal and non-thermal effects(Jung, 2014). Recently, organic solvents including formaldehyde(El Sayed *et al.*, 2016),benzene, tetrahydrofuran, triethylene tetraamine (Maharaz *et al.*, 2018), ethylenediamine (Azodi-Deilami *et al.*, 2014), etc., have been introduced into the preparation of metal chalcogenides. As a result of different properties of the organic solvents including viscosity, polarity, softness ,etc, various synthetic environments could be observed, which would affect the solubility and carrier behaviour of the precursors and as a result, influence the surface morphology and size of the final products (Talebian *et al.*, 2013). At present time, only a few literatures have reported the microwave irradiation synthesis of PbS nanocrystals in various solvents. Qiao et al. reported the preparation of nanocrystalline PbS in ethanol by employing gamma-radiation method (Kuljanin-Jakovljević *et al.*, 2017). The use of microwave irradiation to research fiels have demonstrated very rapid growth due to its particular reaction effects includes rapid volumetric heating and the indirect dramatic increase in reaction rates, etc. PbS has been used in various applications such as light-emitting diodes, infrared detectors, optic fibers, infrared lasers, solar energy panels, window coatings, and environment as Pb^{2+} sensors (Chen *et al.*, 2016). This large panel of applications is due to its interesting physical properties. In addition, PbS has a large Bohr exciton radius (18nm), small effective electron and hole masses ($m_e^* = m_h^* = 0.085m_e$), a large optical dielectric constant ($\varepsilon_\infty = 17.2$)and an infrared direct band gap in the bulk state (0.41 eV at 298 K), which corresponds to an absorption onset at 3024 nm (Souici *et al.*, 2009). In the near-infrared, PbS has a good photoconductive properties.In this work, we report a straight forward analysis on the surface morphology and optical properties of PbS nanostructure in various solvents under the microwave irradiation.

Experimental

Materials and instruments

Lead (II) acetate trihydrates [$(CH_3COO)_2Pb.3H_2O$](MW 379.33g/mol, 99.0%) and thioacetamide (CH_3CSNH_2) (MW: 75.13g/mol, 99.0%) were used as lead and sulphur sources respectively. Ethylene alcohol (C_2H_5OH) was used as a solvents. Lead acetate was purchased from R & M Chemical, thioacetamide from Sigma–Aldrich and solvents from ALFA Chemical Co. All chemicals are analytical grade products and used without further purification.

Synthesis and Characterization

In typical synthesis, 0.01g of lead acetate was added into glass beaker of 500 ml containing 40 ml of aqueous sulphur solution (ethylene glycol and thioacetimade) and magnetically stirred at 500 rpm for 30 min so as obtained homogeneous solution. The beakers were placed in a high power microwave oven (300 W, 2.45 GHz) operated using a pulse regime with 20% power. The reactions were carried out at 10, 15, 45 and 50 min irradiation time, respectively. The precipitates were centrifuged (3500 rpm, 5 min) and washed for with deionized water repeatedly. The dark brown products were obtained and dried in a vacuum oven at 60℃. During the process, microwave irradiations provides the energy for the decomposition with accelerating the nucleation of nanoparticles and depress the growth of the new form of PbS nuclei due to the collisions of the molecules created and the intense friction. The reaction process for forming PbS nanoparticles in ethylene alcohol depends on high temperature which decompose thioacetamide and release S^{2-}ions homogeneously which promoting high rate of nucleation and growth of PbS nanoparticles according to the following chemical reaction;

$$CH_3CSNH_2 \rightarrow CH_3CN + H_2S(1)$$

$$H_2S + Pb(A_c)_2 \rightarrow PbS(nanoparticles) + 2HA_c(2)$$

Equation (1) represents that the decomposition of thioacetamide (CH_3CSNH_2) by microwave heating. CH_3CNandH_2S would be formed. Then further H_2S reacts with $Pb(A_c)_2$ to give PbS nanoparticle. Equation (2) shows the result. Fig 1 represents the schematic of the formation of PbS nanoparticles. The final products were characterized by X-ray diffraction (XRD) at a scanning rate of 5^o/min in the 2θ range 20–70° using a Philips X-ray diffractometer (7602 EA Almelo) with Cu Kα radiation (λ = 0.1542 nm). The particle size and size distribution were determined from the transmission electron microscopy (TEM) micrographs (HTACHI H-7100 TEM). The TEM characterization was carried out at 100 keV. The optical properties of PbS nanoparticles were characterized using UV–visible absorption spectroscopy (UV-1650PC SHIMADZU).

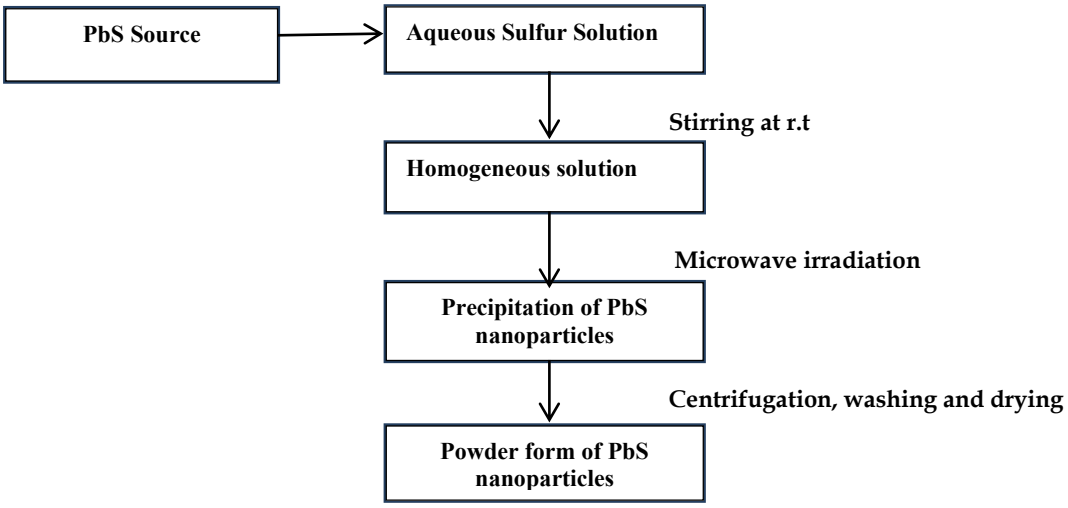

Figure 1. A schematic of the formation of PbS nanoparticles

RESULTS AND DISCUSSION

Figure 2 show The X-ray diffraction pattern for the four samples of PbS nanoparticles irradiated at 10, 15, 45 and 50 min, respectively. The diffraction peaks indicate the nanocrystalline nature with peaks at angles (2θ) of 30.085, 25.978, 43.066, 50.985, 70.949, 53.427, 78.948, 68.894 and 62.541correspond to the reflection from: (111), (200), (220), (311),(222), (400), (331), (420), and (422) crystal planes which can be filed to the structure of pure cubic lead sulphide (ICDD PDF 96-900-8695) with 5.93 A° as lattice parameter, respectively. No detected peaks from the impurities which confirmed the samples high purity. In these samples (200) plane is very clear and abundant which indicates preferential growth of crystallites in this particular direction. The average crystal sizes (D) were calculated based on the width of the peak due to (200) planes by using the Scherrer's formula (Kurmude *et al*., 2014).

$$D = \frac{0.94\lambda}{Cos\theta} \qquad (3)$$

Where λ is the wavelength of X-ray used, C is the full width at half maximum (FWHM) and θ is the Bragg's angle of reflection. The average crystalline size (Table 1) calculated from eq (3) implies that the crystalline size of nanoparticles decreases with increasing dipole of the solvents corresponds to the increases of XRD peaks broadening (FWHM).Figure 3 exhibits the TEM images ofthe nanoparticle sizes and shapes, respectively. It can also be seen from this Figure at 10 and 15 min irradiation time, the particles are in spherical forms with less than 50 nm sizes, while increasing the irradiation time to 20 and 30 min, the particles sizes held together and assembled into flower-like products (Figures 3) while at 45and 50 min irradiation time, the PbS particles with dendritic structure are obtained. From these images, the result shows that, the individual dendrite of PbS is made up of trunks and branches. The result also shown that the individual PbS dendrite has six trunks distributed along 3-D symmetric axis directions and 4 rows of branches which symmetrically stand on each trunk. The branches in each trunk are parallel to each other and in the same plane. Dendrites have enticing applications in sensors, optical and electronic systems, and fluorescence enhancement materials (Lu *et al*., 2006). To the best of our knowledge, the TEM Image of

PbS branches with quadrangle cross section are proved for the first time synthesized using ethylene alcohol. However, a PbS dendrite result was obtained using chemical method (Salavati-Niasari and Ghanbari, 2012).

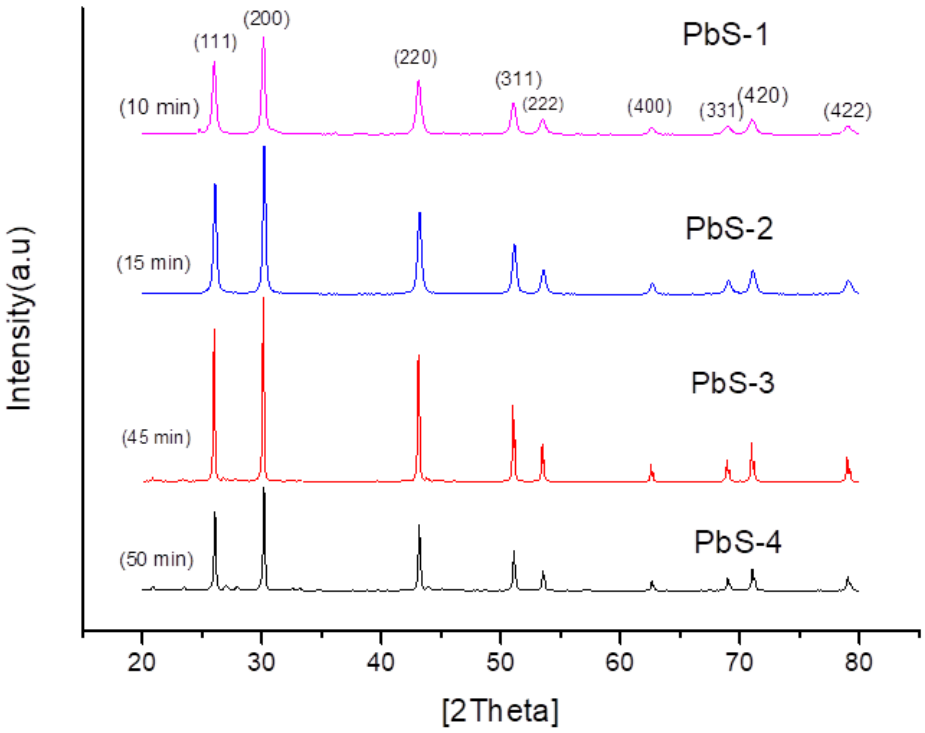

Figure2. X-ray diffraction patterns of PbS nanoparticles prepared at 10, 15, 45 and 50 min.

Table1: X-ray diffraction results of PbS nanoparticles

Samples	Irradiation Time(min)	FWHM of (200)(2θ)	Intensity of (200)(2θ)	Average particle size XRD (nm)
PbS-1	10	0.35199	11565.616	39.2
PbS-2	15	0.28584	17821.778	46.5
PbS-3	45	0.18794	12043.605	65.3
PbS-4	50	0.16118	21776.481	65.8

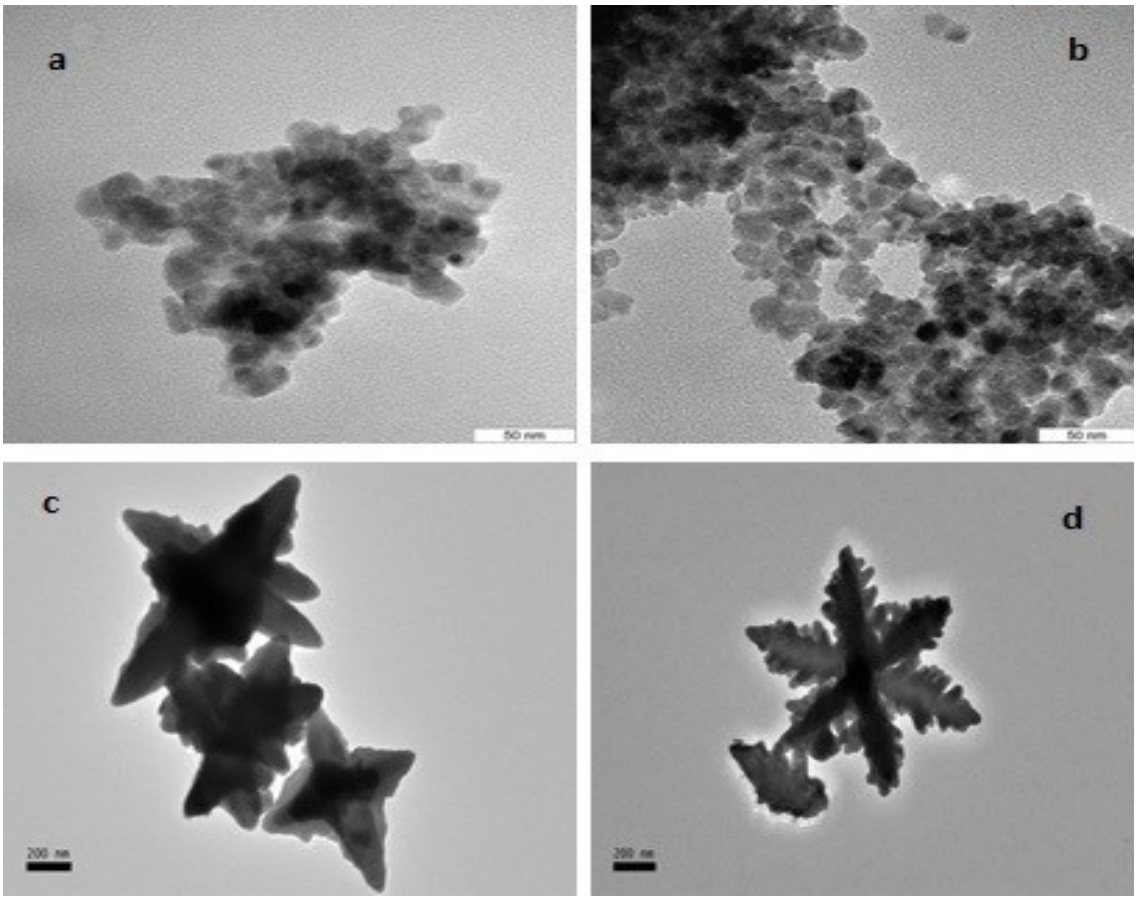

Figure 3.The TEM Images of as-prepared PbS nanoparticles at different irradiation time: (a) 10 (b) 15 (c) 20 and (e) 30 min

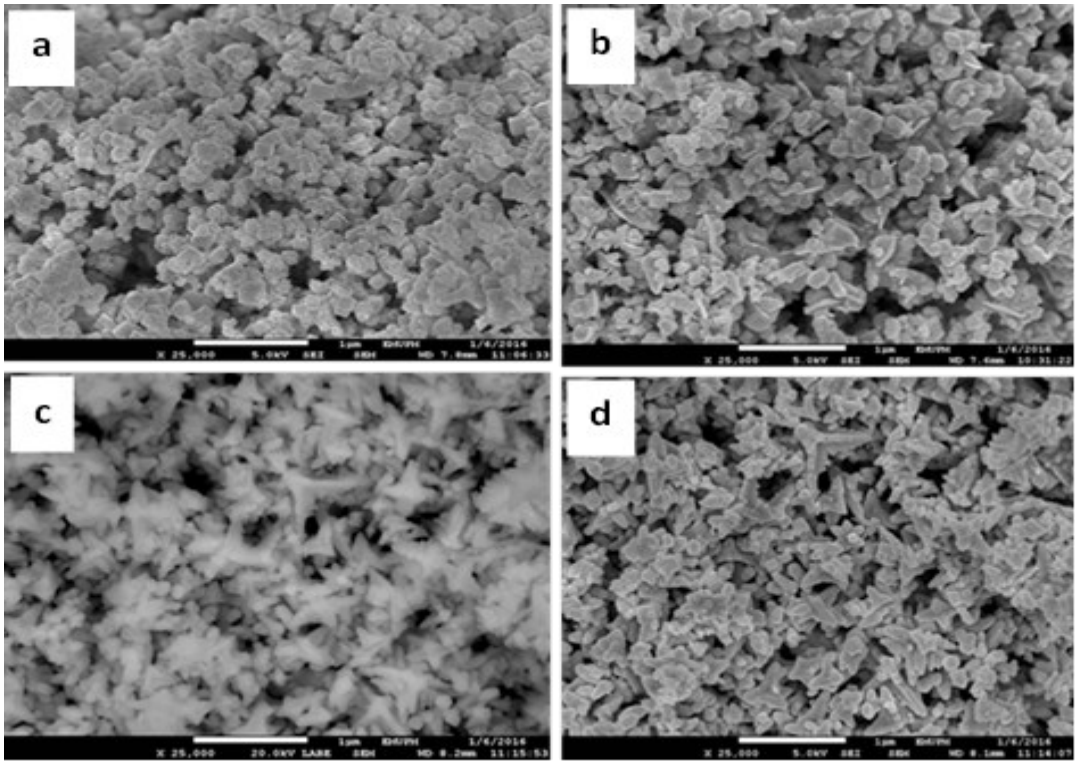

Figure 4.The FESEM Images of as-prepared PbS nanoparticles at different irradiation time: (a) 10 (b) 15 (c) 45 and (e) 50 min.

The FESEM images of PbS nanoparticles synthesized in different irradiation time of 10, 15, 45 and 50 min are shown in Figure 4. It is evident from these images, the surface morphology are not densely packed in some portions this may be due to the effect of solvent used during washing step which can affect the morphological characteristic of the final product. It also evident that the size and shape of the nanoparticles were changed apparently with increases in irradiation time which causes a gradual change in surface morphology. Moreover, when the irradiation time was set to 50 min, the generation of agglomerates makes the system not homogeneous and not well dispersed like the other obtained at 10 min.From the UV-vis absorption study, the optical band gaps of the nanoparticles were estimated which is corresponds to the transition from valence bands to the conduction bands using the following equation:

$$\alpha(v) = A\left(hv/2 - E_g\right)^{m/2} \qquad (4)$$

Where α is the absorption coefficient, A a constant related to the material properties, hv represent the energy of a photon, E_g the optical band gap and m equals 1 for a direct transition. The two peaks were observed from the absorbance spectrum of the sample, the weaker peak at around 250 nm and the higher observed at around 550 nm. Both the two peaks can be assigned to the exciton transitions. The energy intercept of a plot of $\left(\alpha E_{phot}\right)^2$ versus E_{phot} yields E_g for a direct transition (Figure 5) (Zhao *et al.*, 2004). The band gap energies of PbS nanoparticles at different irradiation are listed in table 2, respectively. Among the four samples, the PbS synthesized at 10 min (PbS-1) obtained the

smallest particle size with higher band gap energy which is greater than 0.41eV for bulk PbS semiconductor. The dependence of the energy of electron transitions between quantized levels of the valance and conduction bands on the particle size was used to estimate the particle size.Such transition is often called excitonic, because an electron-hole pair generated by light absorption is similar to the Wannier-Mott exciton in a bulk crystal. The decrease in particle size with increase in band gap energy of as-prepared PbS nanoparticles is signifying the size quantization effects(Song *et al.,* 2014). Size quantization of charges in a small volume crystallite is well known to form the blue shift.The corresponding values of blue shift energies of the samples are listed in table 2.

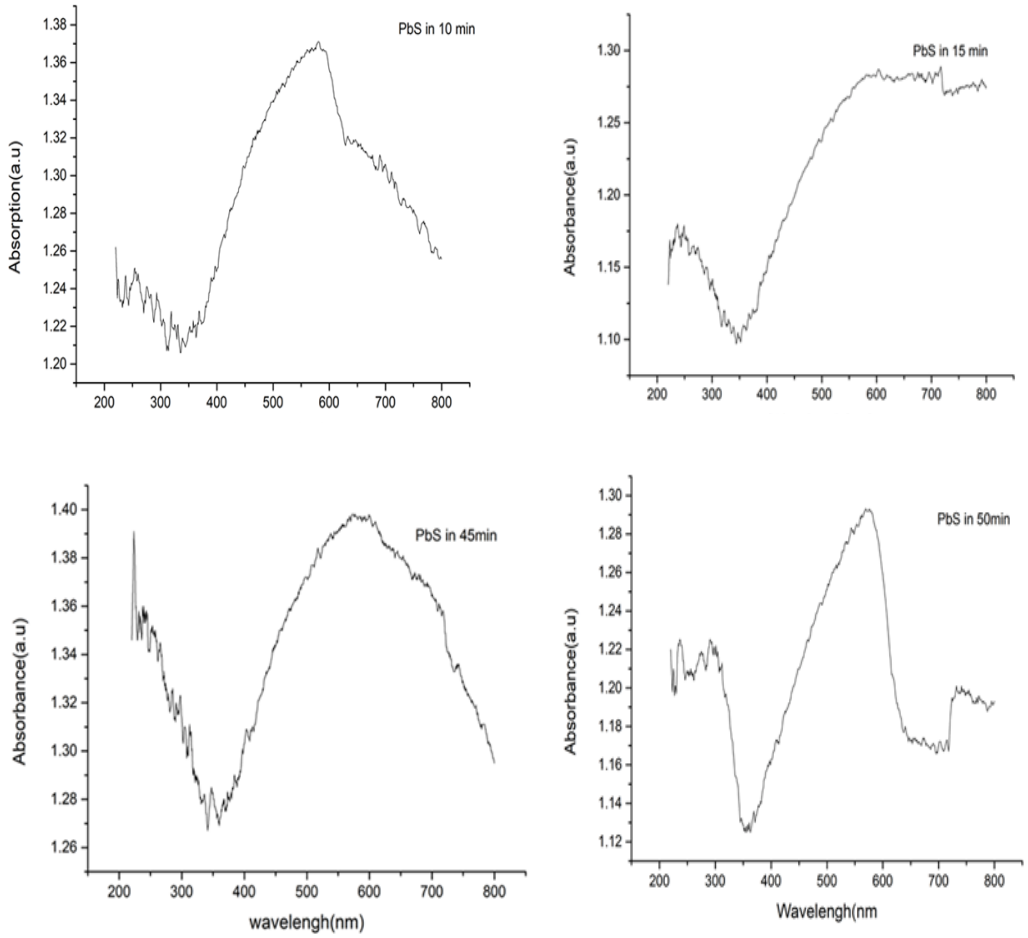

Figure 5. The UV–vis absorbance spectrum of PbS nanoparticles prepared at 10, 15, 45 and 50 min irradiation time.

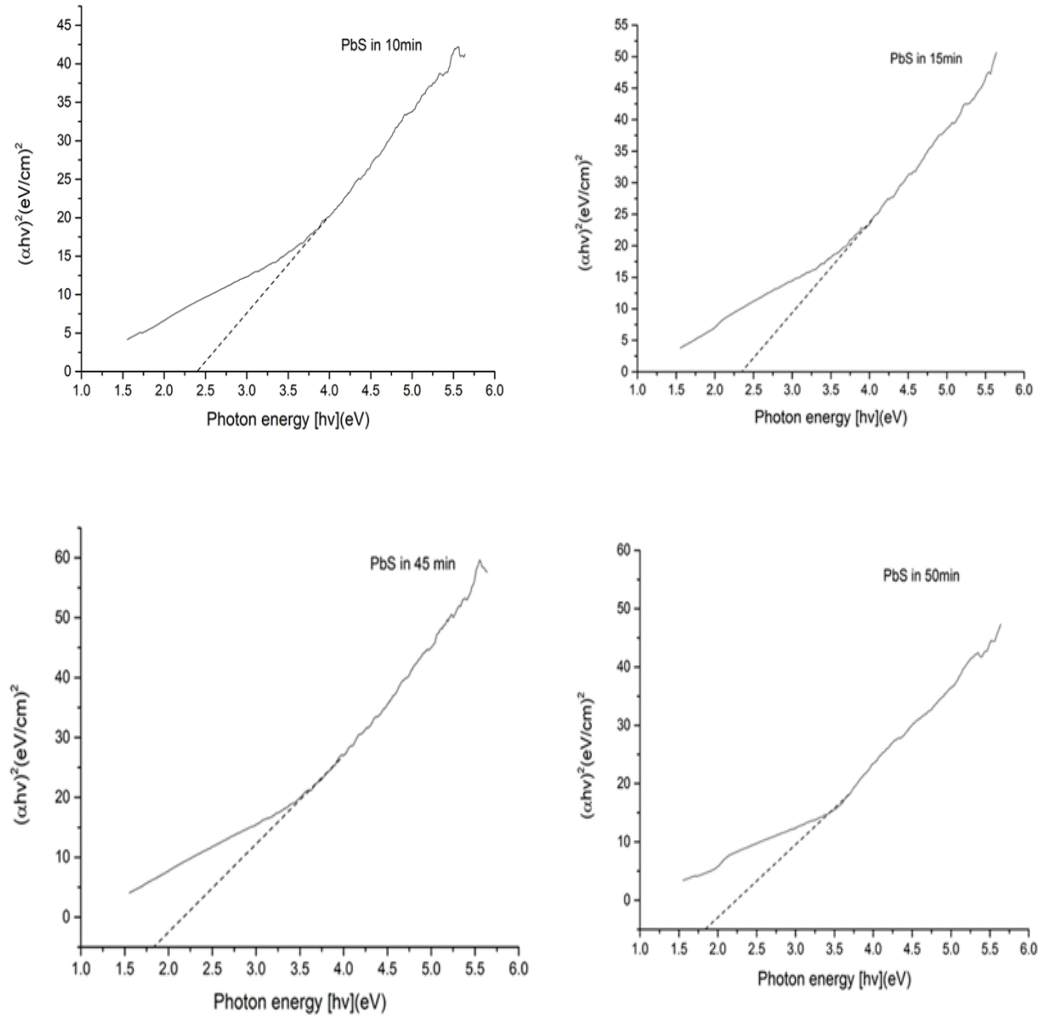

Figure 6. Plot of $(\alpha E_{phot})^2$ vs. E_{phot} for direct transitions of as prepared PbS nanoparticles at 10, 15, 45 and 50 min irradiation time.

Table 2. Band gap energies, blue shift and shape of the particles

Samples	Irradiation time(min)	Band gap (eV)	ΔE (eV)	Shape of particles
PbS-1	10	2.41	2.0	nanoparticles
PbS-2	15	2.36	1.95	nanoparticles
PbS-3	45	1.61	1.41	Dendritic
PbS-4	50	1.60	1.19	Dendritic (perfect)

The result from Table 2 shows that the band gap energy decreases with the increase in the irradiation time; this is related to the particle sizes of the samples. The smaller the particle size, the larger the band gap of the samples due to the quantum conferment effect of the samples. This result clearly shows that a longer irradiation time influences Ostwald ripening due to its effect on the interfacial energy, growth rate coefficients, and solubility which can increase the particle size. The microwave quantum energy is much less than the ionization energies of the compounds. This energy can act as non–ionizing radiation that causes the molecular motions of the ions and the rotation of the dipoles but it does not affect the molecular structure.

Conclusion

Lead sulfide nanoparticles with different particle sizes have been successfully synthesized using various solvents under microwave irradiation method using as $CH_3COO)_2Pb.3H_2O$and CH_3CSNH_2 the starting materials. From the UV absorption, a strong blue-shift with decreasing in nanoparticles size was obtained. Therefore, the result of this research indicated that the smaller the particle size the larger the band gap of the samples due to the quantum conferment effect of the samples. The surface morphology of the sample was gradually changed with varying irradiation time. This method proved to be simple and efficient as well as the friendship to the environment. A possible mechanism for the reaction was proposed. This approach may be applicable to other materials.

Acknowledgments

The authors appreciate the financial support for the work from University Putra Malaysia (UPM).

References

Azodi-Deilami, S., Abdouss, M., and Kordestani, D. (2014). Synthesis and characterization of the magnetic molecularly imprinted polymer nanoparticles using N, N-bis methacryloyl ethylenediamine as a new cross-linking agent for controlled release of meloxicam. *Applied biochemistry and biotechnology, 172* (6), 3271-3286.

Chen, J., Kong, Y., Feng, S., Chen, C., Wo, Y., Wang, W., Dong, Y., Wu, Z., Li, Y., and Chen, S. (2016). Recycled synthesis of whey-protein-capped lead sulfide quantum dots as the second near-infrared reporter for bioimaging application. *ACS Sustainable Chemistry & Engineering, 4* (6), 2932-2938.

El Sayed, S., Pascual, L. s., Licchelli, M., Martínez-Máñez, R. n., Gil, S., Costero, A. M., and Sancenón, F. l. (2016). Chromogenic detection of aqueous formaldehyde using functionalized silica nanoparticles. *ACS applied materials & interfaces, 8* (23), 14318-14322.

Fuku, K., Hayashi, R., Takakura, S., Kamegawa, T., Mori, K., and Yamashita, H. (2013). The synthesis of size-and color-controlled silver nanoparticles by using microwave heating and their enhanced catalytic activity by localized surface plasmon resonance. *Angewandte Chemie, 125* (29), 7594-7598.

Gomez, J. L., and Tigli, O. (2013). Zinc oxide nanostructures: from growth to application. *Journal of Materials Science, 48* (2), 612-624.

Jung, Y. (2014). *Self-assembly of anisotropic nanostructures.* University of Pittsburgh.

Kango, S., Kalia, S., Celli, A., Njuguna, J., Habibi, Y., and Kumar, R. (2013). Surface modification of inorganic nanoparticles for development of organic–inorganic nanocomposites—a review. *Progress in Polymer Science, 38* (8), 1232-1261.

Kuljanin-Jakovljević, J. Ž., Radosavljević, A. N., Spasojević, J. P., Carević, M. V., Mitrić, M. N., and Kačarević-Popović, Z. M. (2017). Gamma irradiation induced in situ synthesis of lead sulfide nanoparticles in poly (vinyl alcohol) hydrogel. *Radiation Physics and Chemistry, 130*, 282-290.

Kurmude, D., Barkule, R., Raut, A., Shengule, D., and Jadhav, K. (2014). X-ray diffraction and cation distribution studies in zinc-substituted nickel ferrite nanoparticles. *Journal of Superconductivity and Novel Magnetism, 27* (2), 547-553.

Kus, M., Alic, T. Y., Kirbiyik, C., Baslak, C., Kara, K., and Kara, D. A. (2018). Synthesis of nanoparticles *Handbook of Nanomaterials for Industrial Applications* (pp. 392-429): Elsevier.

Lai, C.-H., Lu, M.-Y., and Chen, L.-J. (2012). Metal sulfide nanostructures: synthesis, properties and applications in energy conversion and storage. *Journal of Materials Chemistry, 22* (1), 19-30.

Lu, L., Kobayashi, A., Kikkawa, Y., Tawa, K., and Ozaki, Y. (2006). Oriented attachment-based assembly of dendritic silver nanostructures at room temperature. *The Journal of Physical Chemistry B, 110* (46), 23234-23241.

Maharaz, M., Halimah, M., Paiman, S., Saiden, N., and Alibe, I. (2018). Influence of Solvents and Irradiation time on Structural and Optical Properties of Cubic PbS Nanoparticles. *INTERNATIONAL JOURNAL OF ELECTROCHEMICAL SCIENCE, 13* (10), 9317-9332.

Peng, X., Cheng, K., Kang, J., Gu, B., Yu, X., Zhang, Q., and Wang, Y. (2015). Impact of Hydrogenolysis on the Selectivity of the Fischer–Tropsch Synthesis: Diesel Fuel Production over Mesoporous Zeolite-Y-Supported Cobalt Nanoparticles. *Angewandte Chemie International Edition, 54* (15), 4553-4556.

Rai, P., Kwak, W.-K., and Yu, Y.-T. (2013). Solvothermal synthesis of ZnO nanostructures and their morphology-dependent gas-sensing properties. *ACS applied materials & interfaces, 5* (8), 3026-3032.

Salavati-Niasari, M., and Ghanbari, D. (2012). Hydrothermal synthesis of star-like and dendritic PbS nanoparticles from new precursors. *Particuology, 10* (5), 628-633.

Singh, R., and Mohanty, K. K. (2015). Synergy between nanoparticles and surfactants in stabilizing foams for oil recovery. *Energy & Fuels, 29* (2), 467-479.

Song, X., Wang, M., Deng, J., Ju, Y., Xing, T., Ding, J., Yang, Z., and Shao, J. (2014). ZnO/PbS core/shell nanorod arrays as efficient counter electrode for quantum dot-sensitized solar cells. *Journal of Power Sources, 269*, 661-670.

Souici, A., Keghouche, N., Delaire, J., Remita, H., Etcheberry, A., and Mostafavi, M. (2009). Structural and optical properties of PbS nanoparticles synthesized by the radiolytic method. *The Journal of Physical Chemistry C, 113* (19), 8050-8057.

Taglietti, A., Arciola, C. R., D'Agostino, A., Dacarro, G., Montanaro, L., Campoccia, D., Cucca, L., Vercellino, M., Poggi, A., and Pallavicini, P. (2014). Antibiofilm activity of a monolayer of silver nanoparticles anchored to an amino-silanized glass surface. *Biomaterials, 35* (6), 1779-1788.

Talebian, N., Amininezhad, S. M., and Doudi, M. (2013). Controllable synthesis of ZnO nanoparticles and their morphology-dependent antibacterial and optical properties. *Journal of Photochemistry and Photobiology B: Biology, 120*, 66-73.

Wise, F. W. (2000). Lead salt quantum dots: the limit of strong quantum confinement. *Accounts of Chemical Research, 33* (11), 773-780.

Yamamoto, E., and Kuroda, K. (2016). Colloidal mesoporous silica nanoparticles. *Bulletin of the chemical society of Japan, 89* (5), 501-539.

Zhao, Y., Liao, X.-H., Hong, J.-M., and Zhu, J.-J. (2004). Synthesis of lead sulfide nanocrystals via microwave and sonochemical methods. *Materials chemistry and physics, 87* (1), 149-153.